tvst

Article

Intravital Imaging of Circulating Red Blood Cells in the Retinal Vasculature of Growing Mice

Jehwi Jeon[1,2], Yoonha Hwang[2,3], Jingu Lee[2,3], Eunji Kong[1,2], Jieun Moon[2,3], Sujung Hong[2,3], and Pilhan Kim[1–3]

[1] Graduate School of Medical Science and Engineering, Korea Advanced Institute of Science and Technology (KAIST), Daejeon, Republic of Korea
[2] KI for Health Science and Technology, Korea Advanced Institute of Science and Technology (KAIST), Daejeon, Republic of Korea
[3] Graduate School of Nanoscience and Technology, Korea Advanced Institute of Science and Technology (KAIST), Daejeon, Republic of Korea

Correspondence: Pilhan Kim, Graduate School of Medical Science and Engineering, Graduate School of Nanoscience and Technology, KI for Health Science and Technology, Korea Advanced Institute of Science and Technology (KAIST), 291 Daehak-ro, Yuseong-gu, Daejeon, 34141, Republic of Korea. e-mail: pilhan.kim@kaist.ac.kr

Received: February 17, 2021
Accepted: March 21, 2021
Published: April 27, 2021

Keywords: intravital; microscopy; retina; RBC; velocity

Citation: Jeon J, Hwang Y, Lee J, Kong E, Moon J, Hong S, Kim P. Intravital imaging of circulating red blood cells in the retinal vasculature of growing mice. Transl Vis Sci Technol. 2021;10(4):31, https://doi.org/10.1167/tvst.10.4.31

Purpose: To establish a custom-built, high-speed 90 frame-per-second laser-scanning confocal microscope for real-time in vivo retinal imaging of individual flowing red blood cells (RBCs) in retinal vasculature of live mouse model.

Methods: Fluorescently labeled RBCs were injected into mice of different ages (3 to 62 weeks old). Anti-CD31 antibody conjugated with Alexa Fluor 647 was injected to visualize retinal endothelial cells (ECs). Longitudinal and cross-sectional intravital retinal imaging of flowing RBCs and ECs was performed in two strains (C57BL/6 and Balb/c) by using the custom-built confocal microscope.

Results: Simultaneous tracking of the routes of many fluorescently labeled individual RBCs flowing from a large artery and vein to a single capillary in the retina of live mice was achieved, which enabled in vivo measurement of retinal RBC flow velocities in each vessel type in growing mice from 3 to 62 weeks after birth. Average RBC flow velocities were gradually increased during growing from 3 to 14 weeks by more than two times. Then the average RBC flow velocity was maintained at about 20 mm/s in artery and 16 mm/s in vein until 62 weeks.

Conclusions: Our study successfully established a custom-built high-speed 90-Hz retinal confocal microscope for measuring RBC flow velocity at the single cell level. It could be a useful tool to investigate the pathophysiology of various retinal diseases associated with blood flow impairment.

Translational Relevance: This technological method could be a valuable assessment tool to help the development of novel therapeutics for retinal diseases.

Introduction

The eye is one of the most specialized sensory organs in the body. The retina is the innermost thin layer of tissue in the eye, housing numerous photoreceptor cells to convert photons into an electrical signal transmitting to the visual cortex in the brain by the optic nerve for visual recognition.[1] To properly perform its vital function for vision, the retina consumes a large amount of nutrients and oxygen.[2,3] The eye is densely vascularized to maintain the required blood circulation to sufficiently support this high level of metabolic activity.[4] Therefore, failure of the proper blood supply for the retina is one of most major causes in various retinal diseases, especially in vasculopathy such as diabetic retinopathy and retinal vein occlusion.[5–8] Notably, these types of retinal vasculopathies are becoming a primary cause to visual loss in developed countries.[9,10] Recently, increasing evidence has suggested that progression of these vasculopathies is closely related with blood flow.[9–18] In particular, impairment of the retinal blood flow is one of the most important factors for the prognosis and progression monitoring of several retinal disease such as diabetic retinopathy.[13] Accurate and quantitative

measurement of the blood flow in the retinal vasculature can provide valuable information to improve our understanding of the pathophysiology of retinal vasculopathy.[9,10,12,19,20] Several clinical trials have used the retinal blood flow as a diagnostic biomarker for retinal vasculopathy based on clinically available instruments, including Doppler ultrasonography,[20,21] Doppler optical coherence tomography (OCT),[9,10,22] OCT angiography,[12,17,23] and laser speckle flowgraphy.[16,18]

Yet, the outcome of these trials remains unclear in determining the disease progression partly due to the technical limitation in the comprehensive measurement of the retinal blood flow not only in large vessels but also in a small capillary. Most of the currently available instruments analyze only the total blood flow in large arteries and veins, not being able to quantitatively measure the blood flow in the capillary at the single red blood cell (RBC) level.[24] Recent work based on high-speed resonant scanner and adaptive optics clearly demonstrates the capability of quantitative measurement of blood flow in a small capillary to large vessels in the retina of a mouse model by single-cell blood flow imaging.[25–28] However, still, a simultaneous measurement of a single-cell-level blood flow from large vessels to a small capillary in the retina of a small animal model remains technically challenging.

In this study, we implemented a custom-built, high-speed, multicolor confocal microscopy system capable of imaging a single RBC flowing in the retinal vasculature in live mice in vivo with an acquisition speed of 90 frames per second (fps). An individual fluorescently labeled RBC flowing from the artery to the vein through the capillary visualized by in vivo fluorescence labeling of the endothelial cell was successfully imaged, and its velocity was quantitatively analyzed. The changes in the retinal blood flow velocity of large vessels and the capillary in growing mice with an age of 3 to 62 weeks were longitudinally monitored. The established method can be a highly useful tool to investigate the complex pathophysiology of various ocular diseases.

Materials and Methods

Custom-Built High-Speed Laser-Scanning Retinal Confocal Microscopy

Figure 1a shows the schematic of a custom-design laser-scanning confocal microscopy system modified for retina imaging through the mouse crystalline lens in vivo based on previous design.[29–32] Excitation laser beam paths were shown by solid lines, and emitted fluorescence beam paths were shown by dashed lines. Three continuous-wave laser sources, composed of a 488-nm diode laser module (MLD488; Cobolt AB, Stockholm, Sweden), 561-nm DPSS laser (Jive; Cobolt), and 640-nm diode laser module (MLD640; Cobolt), were used as excitation light sources. Laser beams from laser modules were expanded by telescopes consisting of an achromatic lens with focal lengths of 45 mm and 125 mm for a 561-nm wavelength laser beam (L1: #47-636, L2: #47-642; Edmund Optics, Barrington, New Jersesy, USA) or 45 mm and 150 mm for 488-nm and 640-nm wavelength laser beams (L3, L5: #47-636, L4, L6: #47-643; Edmund Optics). Intensity of each laser was independently adjusted by a continuously variable neutral density filter (NDC-50C-4M-A; Thorlabs Inc., Newton, New Jersey, USA). All three laser beams were combined by using dichroic beam splitters (DBS1; FF593-Di03, DBS2; FF520-Di02; Semrock Inc., Rochester, New York, USA) and then delivered to a beam scanner by a multiedge dichroic beam splitter (DBS3; Di01-R405/488/561/635; Semrock). Two-dimensional Raster scanning at 90 Hz was achieved by the beam scanner composed of a rotating 72-facet enhanced aluminum-coated polygonal mirror (SA24; Lincoln Laser, Phoenix, Arizona, USA) for fast-axis scanning and a galvanometer mirror scanner (6230H; Cambridge Technology, Bedford, Massachusetts, USA) for slow-axis scanning. To implement telecentric scanning system, achromatic lenses with effective focal lengths of 50 mm (L7: #47-637; Edmund Optics), 75 mm (L8, L10: #47-639; Edmund Optics), 75 mm with an aperture of 2 inches (L9: #49-292; Edmund Optics), and 125 mm (L11: #47-642; Edmund Optics) were used. Finally, the scanning laser beams were focused by the crystalline lens in the eye of an anesthetized mouse and delivered to the retina through a commercial objective lens (PlanApoλ20X, 0.75NA; Nikon Corporation, Tokyo, Japan) as depicted in Figure 1a. The anesthetized mouse was placed on the articulating-base ball stage (SL20; Thorlabs) fixed to the XYZ translation stage (3DMS; Sutter Instrument, Novato, California, USA). Fluorescence signals were collected by the objective lens. Descanned fluorescence signals were separated from the excitation laser beams by the DBS3 and split into three individual fluorescence signals (green, red, and far-red) by dichroic beam splitters (DBS4; FF560-Di01, DBS5; FF649-Di01; Semrock). Each fluorescence signal was detected by a photomultiplier tube (PMT; R9110; Hamamatsu, Shizuoka Prefecture, Japan) through bandpass filters (FF01-525/45, FF01- 600/37, FF01-697/58; Semrock), 75-mm focal-length achromatic lens (L12:

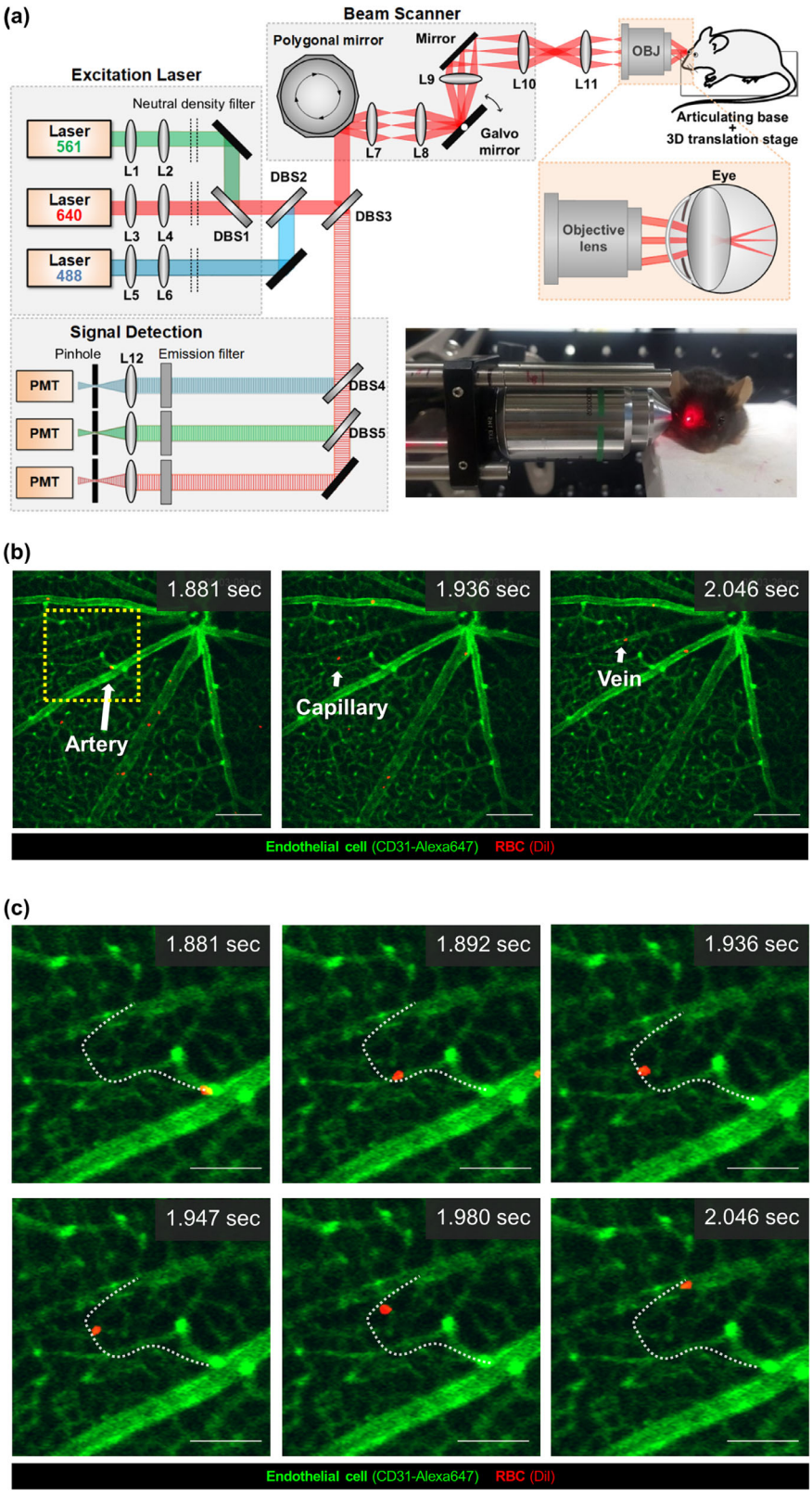

Figure 1. Intravital retinal imaging setup for the tracking of an individual RBC in the retinal vasculature. (**a**) Schematic of the custom-built, high-speed, laser-scanning confocal microscope for intravital retinal imaging through the crystalline lens of a mouse eye. (**b**) Representative intravital images of flowing RBCs (*red*) in the retinal vasculature (*green*). *Scale bars*: 200 µm. (**c**) Magnified images of (**b**) at the region marked by the *yellow dotted box* showing a single RBC flowing from the retinal artery to the vein via the capillary. Tracking of the flowing RBC is shown by the *dotted line*. *Scale bars*: 100 µm.

#47-639; Edmund Optics), and confocal pinholes. Electronic signals from the PMTs were simultaneously digitized by using three-channelframe grabber (Solios; Matrox, Quebec, Canada) with a sampling rate of 29.86 MHz for each channel. Finally, multicolor real-time images with a frame size of 512 by 512 pixels were displayed and recorded at the frame rate of 90 Hz by a custom-developed imaging software using Matrox Imaging Library (MIL9; Matrox).

Animal Model

All animal experiments were approved by the Institutional Animal Care and Use Committee of Korea Advanced Institute of Science and Technology (KAIST) (approval No. KA2019-21). All animals were treated, maintained, and sacrificed in accordance with the policies specified in the ARVO Statement for the Use of Animals in Ophthalmic and Vision Research. Mice were housed and bred in an institutional animal facility in KAIST. All mice were individually housed in ventilated and temperature- and humidity-controlled cages (22.5°C, 52.5%) under a 12/12-hour light/dark cycle and provided with standard diet and water ad libitum. For experimental use, C57B6/N and BALB/c mice were purchased from OrientBio (Suwon, Korea). All imaging and surgical procedures were performed under anesthesia, and all efforts were made to minimize suffering.

Intravital Retinal Imaging of Flowing RBCs in Retinal Vasculature

For in vivo imaging, the mouse was anesthetized with a mixture of zoletil (30 mg/kg) and xylazine (10 mg/kg) by intramuscular injection. Body temperature of the anesthetized mouse was maintained at 36°C by using a homeothermic temperature monitoring and control system (RightTemp; Kent Scientific, Torrington, Connecticut, USA) to prevent the abrupt formation of cold cataract hampering the imaging of retina. Yohimbine (2 mg/kg), antagonist of xylazine, was injected to rescue corneal reflex (blinking reflex) to provide protection from corneal injury or dryness during postanesthesia recovery and stabilization of cardiovascular systems. While corneal reflex was maintained, no spontaneous blinking that disturbed the retinal imaging was achieved. Additional protective measures, including eye ointment and artificial tear to avoid corneal injury, were used with an infrared heating lamp during the recovery state from anesthesia. To visualize the flowing RBCs in the retina, fluorescently labeled RBCs using red fluorophore, DiI (stock no. V-22885; Thermo Fisher Scientific, Waltham, Massachusetts, USA), were intravenously injected (number of RBCs = 4.16×10^7/100 µL) at 12 hours before the intravital imaging. In addition, to simultaneously visualize retinal vasculature, 25 µg anti-CD31 antibody (stock no. 553708; BD Biosciences, Franklin Lakes, New Jersey, USA) conjugated with a far-red color fluorophore, Alexa Fluor 647 (stock no. A20006; Invitrogen, Waltham, Massachusetts, USA), was intravenously injected, which fluorescently labeled endothelial cells of the whole body in a systemic manner. For longitudinal observation of RBC flow velocity changes with aging, intravital imaging of the retina was performed at 3, 4, 8, 14, 18, 22, 32, 42, 60, and 62 weeks old either by repeated imaging of the same mouse or by cross-sectional imaging of individual mice at each time point.

Procedure for Retinal Wholemount

After the intravital retinal imaging, mice were euthanized by using a CO_2 chamber. Both whole eyeballs with optic nerves were carefully harvested by using forceps without tearing and immersed in 1% paraformaldehyde solution for 24 hours for the fixation of entire tissue. After washing the fixed eyeballs with phosphate-buffered saline, they were placed in a small cell culture dish under stereoscopic microscope. Linear incision was made by No. 11 blade at the center of the cornea. Subsequently, a circular incision was performed through the limbus by using iris scissors and the cornea was detached. A single sclerotome was made without damaging retina tissue at the limbus. Crystalline lens, iris, choroid, and sclera were stripped off and the optic nerve was gently cut while avoiding tangential traction damage in the retina. Vitreous body and firmly attached ciliary body were carefully and totally removed from the retina. Finally, the intact retina was flattened on the glass slide for microscopic observation.

RBC Velocity Analysis and Statistical Analysis

Real-time intravital movies of flowing RBCs in retina vasculature were recorded for over 10 seconds with a frame rate of 90 fps using the intravital retinal imaging setup described in the Materials and Methods section. The movies were recorded at two different areas: the temporal and nasal side of the optic disc. All of the recorded movies were extracted to image sequences using ImageJ (National Institutes of Health, Bethesda, MD, USA). To track RBCs flowing in retinal vasculature, individual RBCs were

automatically identified by using the "Spot" function of commercial image analysis software, IMARIS (Bitplane, Belfast, United Kingdom). Typically, the number of automatically identified RBC cells was around 5000 in 900 frames. Tracking of individual RBCs was automatically performed by using the "Spot" function to connect continuously observed RBCs spots over at least three sequential frames. Types of retinal vessels (capillary, artery, vein, and choroid) in which the identified RBCs flowing were categorized by observation of diameter and flowing direction from the optic nerve. Velocity of RBCs was automatically calculated from the RBC tracking results generated by the IMARIS. Statistical analysis was performed by using IBM SPSS Statistics 26.0 (SPSS, Inc., Chicago, IL, USA). Statistical difference was determined by an independent *t*-test and statistical significance was set at *P* values less than 0.05. The mean data of RBC velocities analyzed one-way analysis of variance (ANOVA) followed by post hoc Tukey analysis in different weeks-old age mouse between same strains.

Results

Real-Time Intravital Imaging of the RBC Flow in Retina

Real-time individual RBCs flowing in the retinal vasculature were directly imaged with a custom-built, high-speed, confocal microscopy system[32,33] modified for in vivo retina imaging, shown in Figure 1a. The imaging system can acquire confocal images with a size of 512 by 512 pixels at 90 fps from the retina of a living animal model in vivo. All of the retinal vessel types comprising arteries, veins, and capillaries could be simultaneously visualized in vivo with immunolabeling of endothelial cells by anti-CD31 antibody conjugates shown in Figure 1b. Additionally, individual rapidly flowing fluorescently labeled RBCs in the retinal vasculature could be clearly identified at the same time (Visualization 1 in the supplemental materials). Seemingly difference sizes of flowing RBCs were mostly due to nonuniform fluorescence labeling of individual RBCs. Notably, the artery and vein could be differentiated by the increased level of CD31 labeling in the artery compared to the vein and also by the flowing direction of the RBCs from the optic nerve; the flowing direction of RBCs is away from or toward the optic nerve in the artery and vein, respectively. Figure 1c shows a magnified image of Figure 1b at the region marked by a yellow dotted box showing a single RBC flowing from the artery to the vein via the capillary. The track of the RBC is shown as a white dotted line.

Age-Dependent Change in the Magnification and Axial Length of the Mouse Eye

For in vivo quantification of the RBC flow in the retina of the mouse, the final magnification of the intravital retinal imaging through the crystalline lens in the mouse eye should be accurately measured to determine the actual pixel size. Notably, as shown in Figure 2a, the magnification was significantly changed with the aging of the mice. Yellow circles delineate a similar-sized area in the retina, including the optic disk imaged from mice with different ages of 3 and 22 weeks, showing a decreased refractive power of the crystalline lens with growth. Depending on the refractive power, the angle of views achieved by the intravital retinal imaging setup ranged between 42.83° and 48.05° in C57BL/6 strain mice and 42.68° and 47.62° in Balb/c strain mice at different ages. To calculate the actual pixel size in the intravital retinal imaging, the retina of the same mouse was imaged in vivo through the crystalline lens and then imaged ex vivo after wholemount preparation by standard confocal microscope shown in Figure 2b. The pixel size in the ex vivo imaging by standard confocal microscope was accurately measured to be 1.001 μm with the USAF resolution target. The same microvasculature with distinct branches and bifurcations was identified to calculate the magnification ratio between the ex vivo and in vivo imaging to determine the pixel size in the intravital retinal imaging. This magnification ratio was analyzed around the equator of the retina to avoid peripheral distortion due to substantial spherical aberration of the ball-shaped crystalline lens of mouse eye. The magnification ratios at the different ages were measured in two strains of mice, C57BL/6 and Balb/c, shown in Figures 2c and 2d. Interestingly, the magnification ratio clearly increased after birth until 8 weeks. In older mice aged 14 to 62 weeks, change in the magnification ratio was observed to be much smaller than the initial increase with growing. Additionally, the axial length of the eyeball from the apex of the cornea to the optic nerve entry site of the outer sclera was measured in mice at different ages after birth, shown in Figures 2e–f, demonstrating a similar pattern of growth in both strains: initial increases until 8 weeks followed by gradual increases.

Quantitative Analysis of the RBC Flow Velocity in the Retinal Vasculature With Aging

In this work, to simultaneously visualize the flowing RBCs in the retinal vasculature, a fluorescently labeled

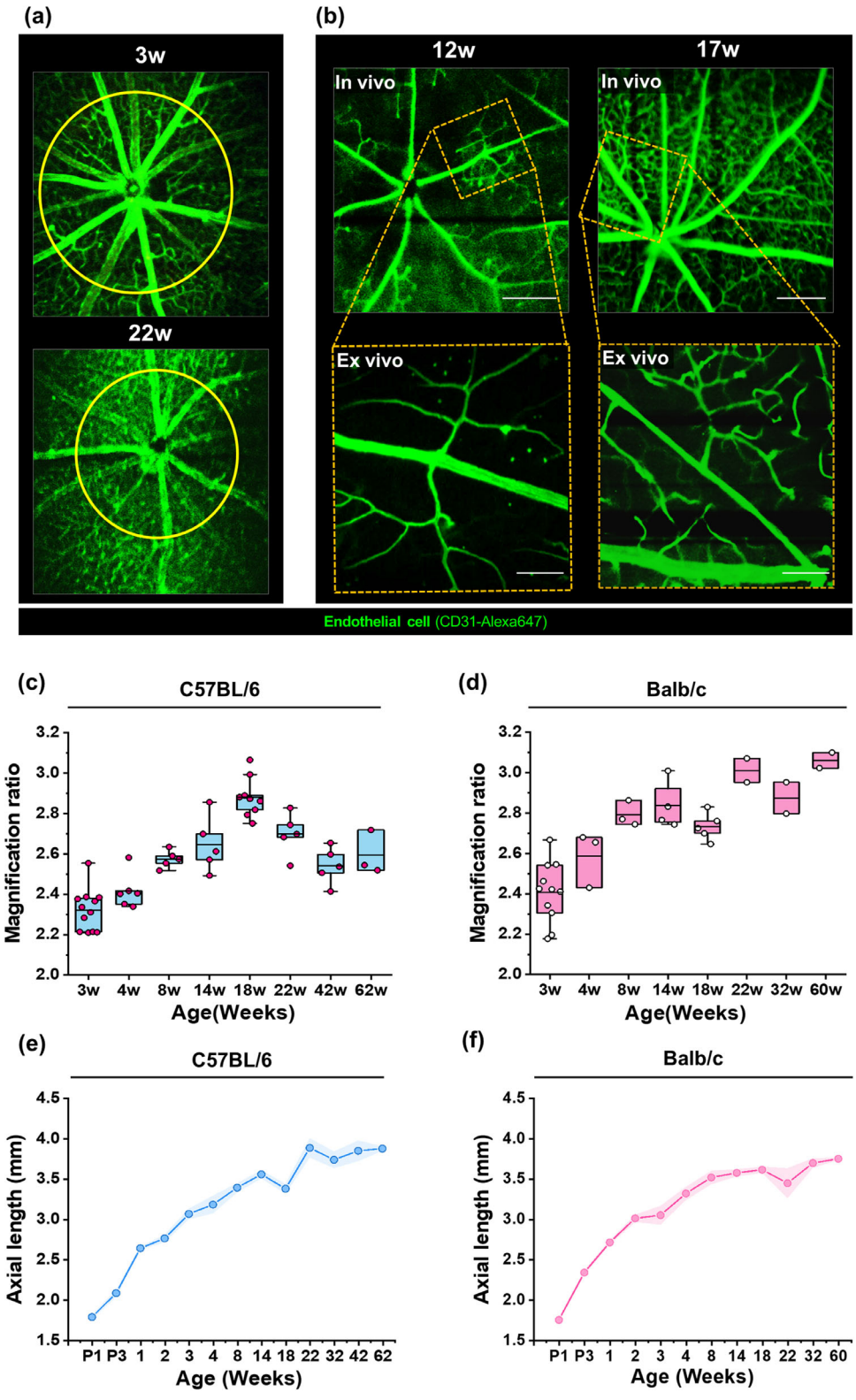

Figure 2. Imaged analysis to quantify the magnification ratio of the intravital retinal imaging of mice at different ages. (**a**) Representative intravital imaging of the retinal vasculature in mice with different ages of 3 and 22 weeks, showing a decreased refractive power of the mouse eye with growth. *Yellow circles* delineate a similar-sized area. (**b**) Representative images of the same retinal vasculature to calculate the magnification ratio between the in vivo and ex vivo imaging at different ages. *Scale bars*: 300 µm in vivo and 100 µm ex vivo. (**c**, **d**) Magnification ratio at different ages of the mice strains of (**c**) C57BL/6 and (**d**) Balb/c, respectively. (**e**, **f**) Axial length of the eyeball changes with aging in the mice strains of (**e**) C57BL/6 and (**f**) Balb/c, respectively. *Shaded area* represents the standard deviation. Number of mice $\geq$3, except 60 and 62 weeks ($n = 2$).

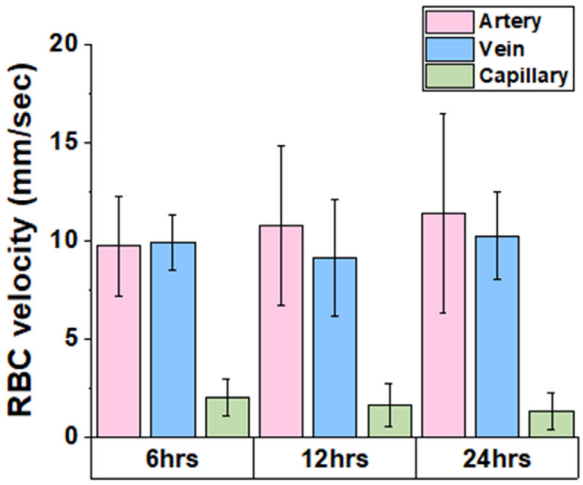

Figure 3. RBC flow velocity measurement after intravenous injection. Comparison of the blood flow velocity measured at 6, 12, and 24 hours after the intravenous injection.

RBC and anti-CD31 antibody conjugate mixture (total volume = 3.5 mL/kg, containing 25 µg CD31) was intravenously injected before the intravital imaging. The increased blood volume in the systemic circulation by the intravenous injection significantly affected the RBC flow in the retinal vasculature. The intravital retinal imaging performed right after the intravenous injection revealed the hampered abnormal flow of RBCs such as tumbling and regurgitation of RBCs in in the artery (Visualization 2 in the supplemental materials), which resulted in an underestimated average RBC flow velocity. Twelve hours after the intravenous injection, the abnormal RBC flows disappeared. In addition, a comparison of the average RBC flow velocity measured at 6, 12, and 24 hours after the intravenous injection showed no statistically significant differences in all types of retinal vessels, arteries, veins, and capillaries, shown in Figure 3.

Utilizing the established methods, the changes of the average RBC flow velocity in the retinal vasculature during growing and aging were evaluated. Figure 4 shows the average RBC flow velocity measured at different ages in two mice strains: C57BL/6 mice aged 3, 4, 8, 14, 18, 22, 42, and 62 weeks and Balb/c mice aged 3, 4, 8, 14, 18, 22, 32, and 60 weeks. The average RBC flow velocity in the retinal artery and vein continuously increased until 14 weeks from 3 weeks after birth by more than two times and then was maintained up to 62 weeks with statistical significance ($P > 0.05$). In the capillary, the average RBC flow velocity was measured to gradually increase until 18 weeks from 3 weeks after the birth, although statistical significance was not achieved as the absolute value of average RBC flow velocity was quite slow (<3 mm/s) even after 18 weeks old. The number of mice was three for every time point except for 60 and 62 weeks ($n = 2$), and the number of tracked RBCs in every vessel was more than 100. After the in vivo imaging, ex vivo imaging was performed to calculate the magnification ratio. In addition to the cross-sectional analysis presented in Figure 4, a longitudinal follow-up measurement of the average RBC flow velocity changes in the same mouse was performed up until 14 weeks from 3 weeks after birth in the two mice strains ($n = 2$) shown in Figure 5 to reconfirm the observation of a significant increase of average RBC flow velocities in the growing mice. As expected, the tendency of the changes and the measured RBC flow velocity from the longitudinal measurement matched with the cross-sectional result from Figure 4, shown in gray in Figure 5.

Additionally, in the retina of Balb/c strain mice with no pigmentation in retinal pigment epithelium cells, we could visualize RBCs flowing in the choroid. Unfortunately, the velocity measurement of the RBCs in the choroid was difficult due to a much smaller number of detected RBCs compared to those in the retinal vessels and multiple photoreceptor degeneration spots with strong autofluorescence. Nevertheless, the measured average RBC flow velocity in the choroid of Balb/c mice was in a similar range of the reported values measured in a human eye by Doppler ultrasonography[34]: ~6.5 mm/s on average, 4.2 mm/s for the end diastolic velocity, and 10 mm/s for the peak systolic velocity, respectively.

Discussion

In this work, we implemented a custom-built, high-speed laser-scanning confocal microscopy system that could acquire confocal images of 512 × 512 pixels at 90 fps from the retina of a live anesthetized mouse in vivo. Notably, it enabled direct simultaneous high-resolution imaging and tracking of individual RBCs flowing in all types of retinal vessels, arteries, veins, and capillaries discriminating individual vessel segments and branches. In comparison, previously reported retinal blood flow imaging techniques based on Doppler ultrasonography, Doppler OCT, OCT angiography, and laser speckle flowgraphy[9,10,12,16–18,20–23] could not measure single-cell-level blood flow in the retinal vasculature. Recent advance of a scanning laser ophthalmoscope has reported successful visualization of single-cell blood flow in the retina of small animal models.[25–28] Notably, by using a confocal scanning laser ophthalmoscope with an imaging frame rate

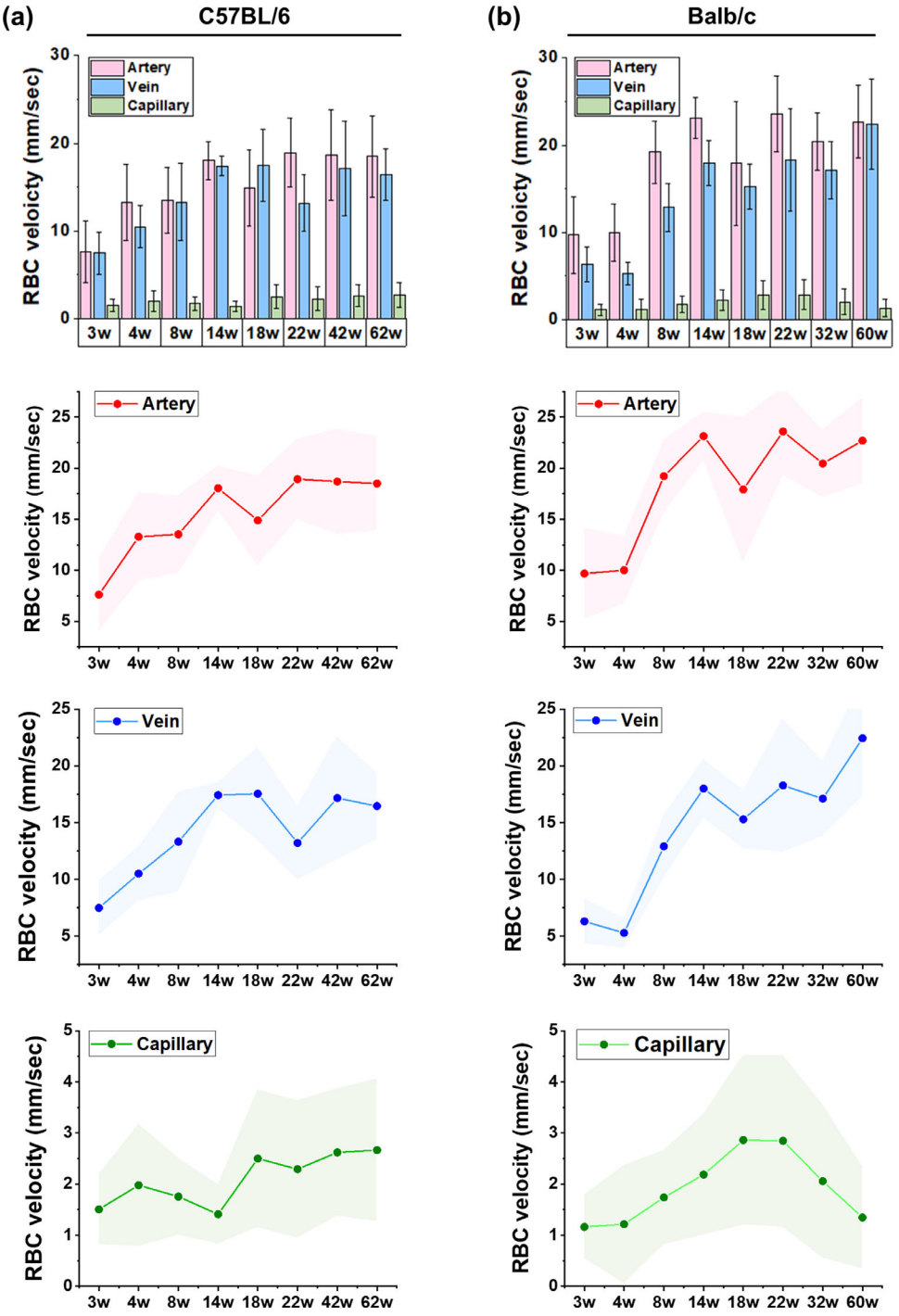

Figure 4. Measurement of the RBC flow velocities in the retinal vessels in mice during aging. (**a**, **b**) RBC flow velocity in the retinal vessels of the artery, vein, and capillary measured at different ages in two mice strains, (**a**) C57BL/6 and (**b**) Balb/c. *Symbols* and *shades* represent the mean value and standard deviation, respectively. The number of mice was 3 for every time point except for 60 and 62 weeks ($n = 2$).

of 25 Hz, in vivo visualization of single blood cell flow and velocity measurement in the mouse retina were reported[28] with high accuracy. However, one-dimensional scanning was performed to quantify the velocity; thus, the measurement was limited to a specific segment of a single vessel at one time point. To the best of our knowledge, our work is the first to visualize and quantify single RBC blood flows simultaneously in the artery, vein, and capillary by two-dimensional confocal imaging of the retina in vivo, which is facilitated by a high imaging frame rate of 90 Hz with a reasonably large number of imaging pixels of

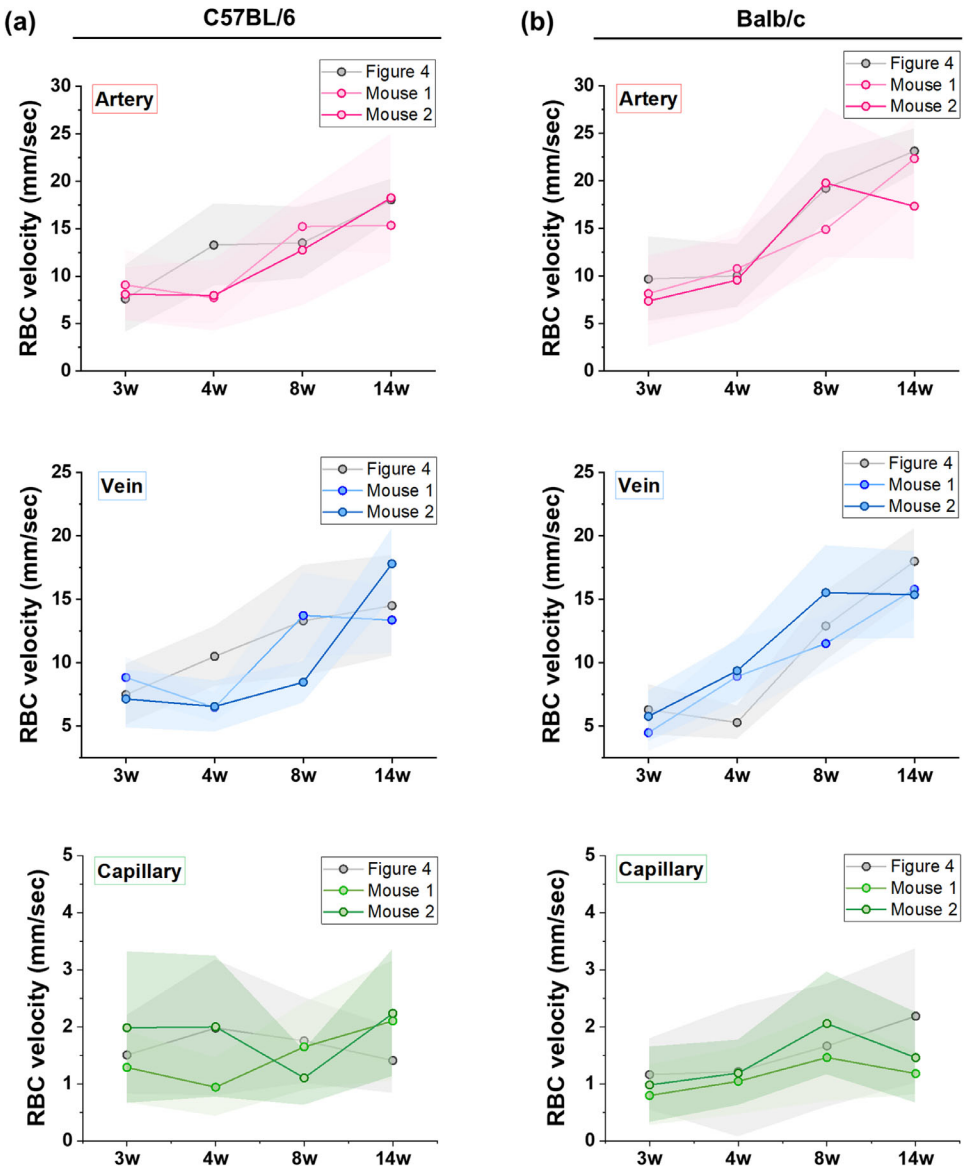

Figure 5. Longitudinal follow-up measurement of the velocity changes in the RBC flow in the same mouse for 14 weeks. (**a**, **b**) The RBC flow velocity in the retinal vessels of the artery, vein, and capillary measured at different ages in the same mice ($n = 2$) with the two strains, (**a**) C57BL/6 and (**b**) Balb/c. For comparison, the cross-sectional measurement results presented in Figure 4 are shown by the *gray lines* with *symbols*. The *symbols* and *shades* represent the mean value and standard deviation, respectively.

512 × 512 per frame to achieve high-resolution imaging enough to identify individual RBCs flowing in retinal vessels (Visualization 1 in the supplemental materials).

Because our imaging method was noncontacting and noninvasive, mice could be fully recovered from the anesthetization after the imaging, enabling longitudinal repetitive in vivo imaging in the same mouse. By virtue of fast two-dimensional imaging of the retina, the total imaging time required for the velocity analysis of all types of retinal vessels, arteries, veins, and capillaries could be reduced to less than 5 minutes acquiring 27,000 frames. It minimizes any potential cornea damage or cataract formation due to tear-film instability, dryness, or other adverse effects by anesthetization, thereby supporting the successful longitudinal repetitive observation of the same mouse over weeks to months, which is highly useful to monitor the progression and treatment efficacy in the mouse models of various retinal diseases. In this work, we successfully achieved longitudinal follow-up imaging of the RBC flow in the same mouse until 14 weeks from 3 weeks after birth, shown in Figure 5.

To the best of our knowledge, the velocity changes of the retinal RBC flow in a growing mouse have

not yet been quantitatively analyzed. In this work, we measured the RBC flow velocity in the retina of mice at different ages from 3 to 62 weeks, shown in Figure 4. Interestingly, the RBC flow velocity in the retinal artery and vein continuously increased until 14 weeks from 3 weeks after birth by more than two times. In contrast, the axial length of the eyeball increased only ~16% during the same time period. We speculated that this relatively large increase in the RBC flow velocity during the growth might be a result of the volumetric growth of the eyeballs associated with vascular maturation, including a decline in the number of vascular branches, length, and area fraction[35,36] while providing a similar level of oxygen and nutrients. In humans, the velocity changes of the retinal blood flow during growth are mostly unknown. Nevertheless, the retinal blood flow velocity in a midage adult measured by Doppler OCT[37] was reported to be 15 to 20 mm/s, almost similar to our measurement of the RBC flow velocity in the large retinal vessels of mice aged 14 to 62 weeks.

Recently, in addition to retinal vessels, there has been increasing interest in the role of choroidal vessels located below the retina in the pathogenesis of several retinal vascular diseases.[38–40] To further improve the accuracy of the RBC flow velocity measurement in deeply located choroidal vasculature below the retina of the mouse, use of a longer wavelength laser as an excitation source such as two-photon microscopy[41] and photoacoustic microscopy[42,43] to improve tissue penetration, integration of adaptive optics,[44] or a deep learning algorithm[45] to improve the imaging quality would be a viable approach to pursue in future studies.

Conclusion

In this work, we implemented a custom-built, high-speed, multicolor confocal microscopy system for intravital retinal imaging of live mice. Direct imaging of rapidly flowing individual RBCs in the retinal vasculature was simultaneously achieved from the large artery and vein to the single capillary level simultaneously. Longitudinal measurement of the RBC flow velocity in the retinal vasculature in growing mice from 3 to 62 weeks after birth was successfully performed by tracking the flowing route and temporal position of the individual RBCs with an experimentally identified imaging magnification ratio using the crystalline lens of the mouse eye at each age. The established noninvasive retinal imaging technique for circulating RBCs at the single cell level could be a useful tool to investigate the pathophysiology of various retinal diseases associated with blood flow impairment in a more detailed manner.

Acknowledgments

The authors thank Ju Hee Back (KAIST) for her technical support.

Supported by the Basic Research Program (2020R1A2C3005694) and Brain Research Program (2016M3C7A1913844) through the National Research Foundation of Korea (NRF) of Korea funded by the the Ministry of Science and ICT, Republic of Korea.

Disclosure: **J. Jeon,** None; **Y. Hwang,** None; **J. Lee,** None; **E. Kong,** None; **J. Moon,** None; **S. Hong,** None; **P. Kim,** None

References

1. Coomer CE, Wilson SG, Titialii-Torres KF, et al. Her9/Hes4 is required for retinal photoreceptor development, maintenance, and survival. *Sci Rep*. 2020;10(1):11316.
2. Sun Y, Smith LEH. Retinal vasculature in development and diseases. *Annu Rev Vis Sci*. 2018;4:101–122.
3. Pournaras CJ, Rungger-Brandle E, Riva CE, Hardarson SH, Stefansson E. Regulation of retinal blood flow in health and disease. *Prog Retin Eye Res*. 2008;27(3):284–330.
4. Nickla DL, Wallman J. The multifunctional choroid. *Prog Retin Eye Res*. 2010;29(2):144–168.
5. Iijima H. Mechanisms of vision loss in eyes with macular edema associated with retinal vein occlusion. *Jpn J Ophthalmol*. 2018;62(3):265–273.
6. Khayat M, Williams M, Lois N. Ischemic retinal vein occlusion: characterizing the more severe spectrum of retinal vein occlusion. *Surv Ophthalmol*. 2018;63(6):816–850.
7. Ip M, Hendrick A. Retinal vein occlusion review. *Asia Pac J Ophthalmol (Phila)*. 2018;7(1):40–45.
8. Hayreh SS. Ocular vascular occlusive disorders: natural history of visual outcome. *Prog Retin Eye Res*. 2014;41:1–25.
9. Srinivas S, Tan O, Nittala MG, et al. Assessment of retinal blood flow in diabetic retinopathy using Doppler Fourier-domain optical coherence tomography. *Retina*. 2017;37(11):2001–2007.
10. Wang Y, Fawzi A, Tan O, Gil-Flamer J, Huang D. Retinal blood flow detection in diabetic patients by

Doppler Fourier domain optical coherence tomography. *Opt Express*. 2009;17(5):4061–4073.
11. Harris NR, Watts MN, Leskova W. Intravital video microscopy measurements of retinal blood flow in mice. *J Vis Exp*. 2013;(82):51110.
12. Palochak CMA, Lee HE, Song J, et al. Retinal blood velocity and flow in early diabetes and diabetic retinopathy using adaptive optics scanning laser ophthalmoscopy. *J Clin Med*. 2019;8(8):1165.
13. Srinivas S, Tan O, Wu S, et al. Measurement of retinal blood flow in normal Chinese-American subjects by Doppler Fourier-domain optical coherence tomography. *Invest Ophthalmol Vis Sci*. 2015;56(3):1569–1574.
14. Zhong Z, Petrig BL, Qi X, Burns SA. In vivo measurement of erythrocyte velocity and retinal blood flow using adaptive optics scanning laser ophthalmoscopy. *Opt Express*. 2008;16(17):12746–12756.
15. Dervenis N, Coleman AL, Harris A, et al. Factors Associated with retinal vessel diameters in an elderly population: the Thessaloniki Eye Study. *Invest Ophthalmol Vis Sci*. 2019;60(6):2208–2217.
16. Shiga Y, Asano T, Kunikata H, et al. Relative flow volume, a novel blood flow index in the human retina derived from laser speckle flowgraphy. *Invest Ophthalmol Vis Sci*. 2014;55(6):3899–3904.
17. Ashraf M, Sampani K, Abu-Qamar O, et al. Optical coherence tomography angiography projection artifact removal: impact on capillary density and interaction with diabetic retinopathy severity. *Transl Vis Sci Technol*. 2020;9(7):10.
18. Calzetti G, Fondi K, Bata AM, et al. Assessment of choroidal blood flow using laser speckle flowgraphy. *Br J Ophthalmol*. 2018;102(12):1679–1683.
19. Burgansky-Eliash Z, Barak A, Barash H, et al. Increased retinal blood flow velocity in patients with early diabetes mellitus. *Retina*. 2012;32(1):112–119.
20. Divya K, Kanagaraju V, Devanand B, Jeevamala C, Raghuram A, Sundar D. Evaluation of retrobulbar circulation in type 2 diabetic patients using color Doppler imaging. *Indian J Ophthalmol*. 2020;68(6):1108–1114.
21. Karami M, Janghorbani M, Dehghani A, Khaksar K, Kaviani A. Orbital Doppler evaluation of blood flow velocities in patients with diabetic retinopathy. *Rev Diabet Stud*. 2012;9(2–3):104–111.
22. Lee B, Novais EA, Waheed NK, et al. En face Doppler optical coherence tomography measurement of total retinal blood flow in diabetic retinopathy and diabetic macular edema. *JAMA Ophthalmol*. 2017;135(3):244–251.
23. Kaizu Y, Nakao S, Arima M, et al. Flow density in optical coherence tomography angiography is useful for retinopathy diagnosis in diabetic patients. *Sci Rep*. 2019;9(1):8668.
24. Nesper PL, Soetikno BT, Zhang HF, Fawzi AA. OCT angiography and visible-light OCT in diabetic retinopathy. *Vis Res*. 2017;139:191–203.
25. Song W, Zhou L, Yi J. Volumetric fluorescein angiography (vFA) by oblique scanning laser ophthalmoscopy in mouse retina at 200 B-scans per second. *Biomed Opt Express*. 2019;10(9):4907–4918.
26. Guevara-Torres A, Joseph A, Schallek JB. Label free measurement of retinal blood cell flux, velocity, hematocrit and capillary width in the living mouse eye. *Biomed Opt Express*. 2016;7(10):4228–4249.
27. Guevara-Torres A, Williams DR, Schallek JB. Origin of cell contrast in offset aperture adaptive optics ophthalmoscopy. *Opt Lett*. 2020;45(4):840–843.
28. Joseph A, Guevara-Torres A, Schallek J. Imaging single-cell blood flow in the smallest to largest vessels in the living retina. *Elife*. 2019;8:e45077.
29. Seo H, Hwang Y, Choe K, Kim P. In vivo quantitation of injected circulating tumor cells from great saphenous vein based on video-rate confocal microscopy. *Biomed Opt Express*. 2015;6(6):2158–2167.
30. Hwang Y, Yoon H, Choe K, et al. In vivo cellular-level real-time pharmacokinetic imaging of free-form and liposomal indocyanine green in liver. *Biomed Opt Express*. 2017;8(10):4706–4716.
31. Park I, Choe K, Seo H, et al. Intravital imaging of a pulmonary endothelial surface layer in a murine sepsis model. *Biomed Opt Express*. 2018;9(5):2383–2393.
32. Lee JY, Hwang Y, Kim JH, et al. In vivo fluorescence retinal imaging following AAV2-mediated gene delivery in the rat retina. *Invest Ophthalmol Vis Sci*. 2016;57(7):3390–3396.
33. Park JR, Choi W, Hong HK, et al. Imaging laser-induced choroidal neovascularization in the rodent retina using optical coherence tomography angiography. *Invest Ophthalmol Vis Sci*. 2016;57(9):OCT331–OCT340.
34. Urs R, Ketterling JA, Yu ACH, Lloyd HO, Yiu BYS, Silverman RH. Ultrasound imaging and measurement of choroidal blood flow. *Transl Vis Sci Technol*. 2018;7(5):5.
35. Ehling M, Adams S, Benedito R, Adams RH. Notch controls retinal blood vessel maturation and quiescence. *Development*. 2013;140(14):3051–3061.

36. Rust R, Gronnert L, Dogancay B, Schwab ME. A revised view on growth and remodeling in the retinal vasculature. *Sci Rep*. 2019;9(1):3263.
37. Wang Y, Lu A, Gil-Flamer J, Tan O, Izatt JA, Huang D. Measurement of total blood flow in the normal human retina using Doppler Fourier-domain optical coherence tomography. *Br J Ophthalmol*. 2009;93(5):634–637.
38. Semeraro F, Morescalchi F, Russo A, et al. Central serous chorioretinopathy: pathogenesis and management. *Clin Ophthalmol*. 2019;13:2341–2352.
39. Gallego-Pinazo R, Dolz-Marco R, Gomez-Ulla F, Mrejen S, Freund KB. Pachychoroid diseases of the macula. *Med Hypothesis Discov Innov Ophthalmol*. 2014;3(4):111–115.
40. Siedlecki J, Schworm B, Priglinger SG. The pachychoroid disease spectrum—and the need for a uniform classification system. *Ophthalmol Retina*. 2019;3(12):1013–1015.
41. Hadoux X, Hui F, Lim JKH, et al. Non-invasive in vivo hyperspectral imaging of the retina for potential biomarker use in Alzheimer's disease. *Nat Commun*. 2019;10(1):4227.
42. Liu W, Yao J. Photoacoustic microscopy: principles and biomedical applications. *Biomed Eng Lett*. 2018;8(2):203–213.
43. Choi W, Park EY, Jeon S, Kim C. Clinical photoacoustic imaging platforms. *Biomed Eng Lett*. 2018;8(2):139–155.
44. Qin Z, He S, Yang C, et al. Adaptive optics two-photon microscopy enables near-diffraction-limited and functional retinal imaging in vivo. *Light Sci Appl*. 2020;9:79.
45. Mansour RF. Deep-learning-based automatic computer-aided diagnosis system for diabetic retinopathy. *Biomed Eng Lett*. 2018;8(1):41–57.